Supplemental material for: Fundamental limits on the rate of bacterial cell division

Nathan M. Belliveau[1,*], **Griffin Chure**[2,3,*], **Christina L. Hueschen**[4], **Hernan G. Garcia**[5], **Jané Kondev**[6], **Daniel S. Fisher**[7], **Julie Theriot**[1,8], **Rob Phillips**[1,9,†]

***For correspondence:**

[*]These authors contributed equally to this work

[1]Department of Biology, University of Washington, Seattle, WA, USA; [2]Division of Biology and Biological Engineering, California Institute of Technology, Pasadena, CA, USA; [3]Department of Applied Physics, California Institute of Technology, Pasadena, CA, USA; [4]Department of Chemical Engineering, Stanford University, Stanford, CA, USA; [5]Department of Molecular Cell Biology and Department of Physics, University of California Berkeley, Berkeley, CA, USA; [6]Department of Physics, Brandeis University, Waltham, MA, USA; [7]Department of Applied Physics, Stanford University, Stanford, CA, USA; [8]Allen Institute for Cell Science, Seattle, WA, USA; [9]Department of Physics, California Institute of Technology, Pasadena, CA, USA; [†]Address correspondence to phillips@pboc.caltech.edu; [*]Contributed equally

Contents

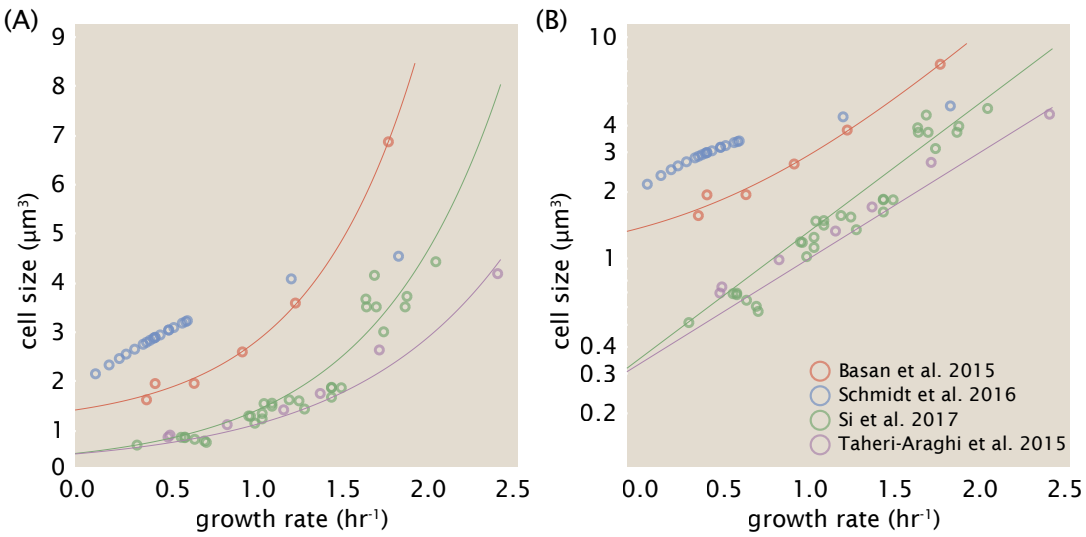

Figure 1. Measurements of cell size as a function of growth rate. (A) Plot of the reported cell sizes from several recent papers. The data in blue come from Volkmer and Heinemann, 2011 (***Volkmer and Heinemann*** (***2011***)) and were used in the work of Schmidt *et al.*. Data from the lab of Terence Hwa are shown in red (***Basan et al.*** (***2015***)), while the two data sets shown in green and purple come from the lab of Suckjoon Jun (***Taheri-Araghi et al.*** (***2015***); ***Si et al.*** (***2017***)). (B) Same as in (A) but with the data plotted on a logarithmic y-axis to highlight the exponential scaling that is expected for *E. coli*.

Summary of Proteome Datasets.

[NB: in progress. I think one useful figure for me to make is a schematic showing how absolute copy numnbers were determined in each paper we considered.]

Summary of final compiled data set.

[NB: in progress]

Adjustments to Schmidt *et al.* dataset

While the dataset from Schmidt *et al.* remains a heroic effort that our lab continues to return to as a resource, there were steps taken in their calculation of protein copy number that we felt needed some further consideration. In particular, the authors made an assumption of constant cellular protein concentration across all growth conditions and used measurements of cell volume that appear inconsistent with an expected exponential scaling of cell size with growth rate that is well-documented in *E. coli* (***Schaechter et al.*** (***1958***); ***Taheri-Araghi et al.*** (***2015***); ***Si et al.*** (***2017***)).

We begin by looking at their cell volume measurements, which are shown in blue in Figure 1. As a compairon, we also plot cell sizes reported in three other recent papers: measurements from Taheri-Araghi *et al.* and Si *et al.* come from the lab of Suckjoon Jun, while those from Basan *et al.* come from the lab of Terence Hwa. Each set of measurements used microscopy and cell segmentation to determine the length and width, and then calculated cell size by treating the cell is a cylinder with two hemispherical ends. While there is a large discrepancy in cell size between the two research groups, Basan *et al.* found that this came specifically from uncertainty in determining the cell width, which is prone to inaccuracy given the small cell size and optical resolution limits (further described in their supplemental text). Perhaps the more concerning point is that while each of these alternative measurements show an exponential increase in cell size at faster growth rates, the measurements used by Schmidt *et al.* appear to plateau. This resulted in an analogous trend in their final reported total cellular protein per cell as shown in Figure 2 (purple data points), and is in disagreement with other measurements of total protein at these growth rates (***Basan et al.*** (***2015***)).

Since it is not obvious how measurements of cell size might have influenced their reported

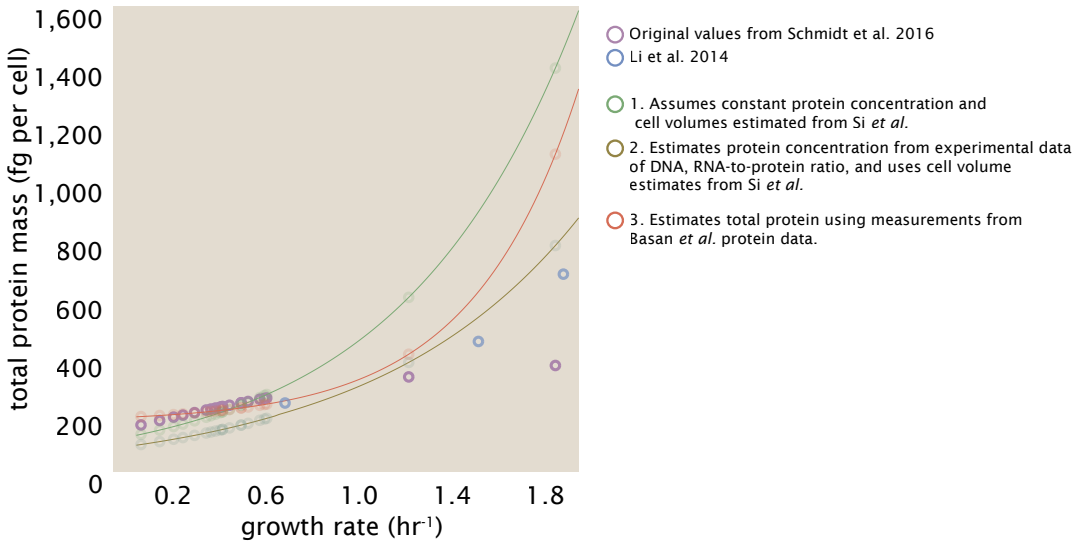

Figure 2. Alternative estimates of total cellular protein for the growth conditions considered in Schmidt *et al.* The original protein mass from Schmidt *et al.* and Li *et al.* are shown in purple and blue, respectively. *Green*: Rescaling of total protein mass assuming a growth rate independent protein concentration and cell volumes estimated from Si *et al.* 2017. *Gold*: Rescaling of total protein mass using estimates of growth rate-dependent protein concentrations and cell volumes estimated from Si *et al.* 2017. *Red*: Rescaling of total protein mass using the experimental measurements from Basan *et al.* 2015.

protein abundances, we will go through this calculation in the next section. We will also show how these can adjusted to better reflect the alternative measurements of cell size shown in Figure 1. Finally, we consider several strategies to adjust the reported copy numbers, with the result summarized in Figure 2. For most growth conditions, we find that total protein expectations are not expected to change dramatically. However, for the fastest growth conditions, with glycerol + supplemented amino acids, and LB media, there is quite a bit of variability among are different estimates.

Effect of cell volume on reported absolute protein abundances in the work of Schmidt *et al.* .

The authors calculated proteome-wide protein abundance by first determining absolute abundances of 41 pre-selected proteins, which relied on adding synthetic heavy reference peptides into their protein samples at known abundance (with proteins selected to cover the range of expected copy numbers). This absolute quantitation was performed in replicate for each growth condition. Separately, the authors also performed a more conventional mass spectrometry measurement for samples from each growth condition, which attempted to maximize the number of quantified proteins but only provided relative abundances based on peptide intensities. Finally, using their 41 proteins with absolute abundances already determined, they then created calibration curves with which to relate their relative intensity to absolute protein abundance for each growth condition. This allowed them to estimate absolute protein abundance for all proteins detected in their proteome-wide data set. Combined with their flow cytometry cell counts, they were then able to determine absolute abundance of each protein detected on a per cell basis.

While this approach provided absolute abundances, another necessary step needed to arrive at total cellular protein is to account for any protein loss during their various protein extraction steps. Here the authors attempted to determine total protein separately using a BCA protein assay. In personal communications, it was noted that determining reasonable total protein abundances by BCA across their array of growth conditions was particularly troublesome. Instead, they noted confidence in their total protein measurements for cells grown in M9 minimal media + glucose

and used this as a reference point with which to estimate the total protein for all other growth conditions.

For cells grown in M9 minimal media + glucose an average total mass of M_P = 240 fg per cell was measured. Using their reported cell volume, reported as V_{orig} = 2.84 fl, a cellular protein concentration of $[M_P]_{orig} = M_P/V_{orig}$ = 85 fg/fl. Now, taking the assumption that cellular protein concentration is relatively independent of growth rate, they could then estimate the total protein mass for all other growth conditions from,

$$M_{P\_i} = [M_P]_{orig} \cdot V_i \tag{1}$$

where M_{P_i} represents the total protein mass per cell and V_i is the cell volume for each growth condition i as measured in Volkmer and Heinemann, 2011. Here the thinking is that the values of M_{P_i} reflects the total cellular protein for growth condition i, where any discrepancy from their absolute protein abundance is assumed to be due to protein loss during sample preparation. The protein abundances from their absolute abundance measurements noted above were therefore scaled to their estimates and are shown in Figure 2 (purple data points).

If we instead consider the cell volumes predicted in the work of Si *et al.*, we again need to take growth in M9 minimal media + glucose as a reference with known total mass, but we can follow a similar approach to estimate total protein mass for all other growth conditions. Letting V_{Si_glu} = 0.6 fl be the predicted cell volume, the cellular protein concentration becomes $[M_P]_{Si} = M_P/V_{Si\_glu}$ = 400 fg/fl. The new total protein mass per cell can then be calculated from,

$$M'_{P\_i} = [M_P]_{Si} \cdot V_{Si\_i} \tag{2}$$

where M'_{P_i} is the new protein mass prediction, and V_{Si_i} refers to the new volume prediction for each condition i, These are shown as [] dots in Figure 2.

Reconsidering assumption that protein concentration is constant.

We next relax the assumption that cellular protein concentration is constant and instead, attempt to estimate it using experimental data. Here we first note that for across almost the entire range of growth rates considered here, protein, DNA, and RNA accounted for at least 90 % of the dry mass in measurements from the lab of Terence Hwa (***Basan et al.*** (***2015***)). They also found that the total dry mass concentration was roughly constant across growth conditions. Under such a scenario, we can calculate the total dry mass concentration for protein, DNA, and RNA, which is given by 1.1 g/ml x 30 % x 90 % or about $[M_P]$ = 300 fg per fl. Using the cell volume predictions from Si *et al.*, we can then calculate the associated mass per cell.

However, even if dry mass concentration is relatively constant across growth conditions, it is not a given that protein concentration should also be constant. In particular, we know that rRNA increases substantially at faster growth rates (***Dai et al.*** (***2016***)). This is a well-documented result that arises from an increase in the fraction of ribosomes at faster growth rates (***Scott et al.*** (***2010***)). To proceed we will use therefore rely on experimental measurements of total DNA content per cell that also come from Basan *et al.*, and RNA to protein ratios that were measured in Dai *et al.* (and cover the entire range of growth conditions considered here). These are reproduced in Figure 3(A) and (B), respectively.

Assuming that the protein, DNA, and RNA account for 90 % of the total dry mass, the protein mass can then determined by first subtracting the experimentally measured DNA mass, and then using the experimental estimate of the RNA to protein ratio. The total protein per cell is will be related to the summed RNA and protein mass by,

$$M_P = \frac{[M_P + M_{RNA}]}{1 + (RP_{ratio})}. \tag{3}$$

(RP_{ratio} refers to the RNA to protein ratio as measured by Dai *et al.*. In Figure 3(C) we plot the estimated cellular concentrations for protein, DNA, and RNA from these calculations, and in Figure 3(D) we plot their total expected mass per cell.

Estimating cellular protein concentration as a function of growth rate.

One of the challenges in our estimates in the preceding sections is the need to estimate protein concentration and cell volumes. These are inherently difficult to to accurately due to the small size of *E. coli*. Indeed, for all the additional measurements of cell volume included in Figure 1, no measurements were performed for cells growing at rates below 0.5 hr^{-1}. It therefore remains to be determined whether our extrapolated cell volume estimates are appropriate, with the possibility that the logarithmic scaling of cell size might break down for slower growth.

In our last approach we therefore attempt to estimate total protein using experimental data that required no estimates of concentration or cell volume. Specifically, in the work of Basan *et al*, the authors measured total protein per cell for a broad range of growth rates (reproduced in Figure 4). These were determined by first measuring bulk protein from cell lysate, measured by the colorimetric Biuret method (***You et al.*** (***2013***)), and then abundance per cell was calculated from cell counts from either plating cells or a Coulter counter. While it is unclear why Schmidt *et al.* was unable to take a similar approach, the results from Basan *et al* appear more consistent with our expectation that cell mass will increase exponentially with faster growth rates. In addition, although they do not consider growth rates below about 0.5 hr^{-1}, it is interesting to note that the protein mass per cell appears to plateau to a minimum value at slow growth. In contrast, our estimates using cell volume so far have predicted that total protein mass should continue to decrease slightly for slower growing cells. By fitting this data to an exponential function dependent on growth rate, we could then estimate the total protein per cell for each growth condition considered by Schmidt *et al.*. These are plotted in red in Figure 2.

Estimation of cell size and surface area.

In Figure 1 we looked at a number of recent cell size measurements and potential issues with the values used by Schmidt *et al.*. Since most of our data sets lacked any cell size measurements, we chose instead to use a common set of size measurements for any analysis that required calculation of cell size or surface area. Here we compile the cell size measurements from the recent works of Si *et al.* 2017, 2019, which covers almost the entire range of growth rates considered across the proteomic data (shown in Figure 5). In each dataset, the authors made measurements on strains MG1655 and NCM3722, which each appear to show a logarithmic scaling with growth rate.

Since each of our proteomic datasets use either K-12 MG1655 or its derivative BW25113 (from the lab of Barry L. Wanner; the parent strain of the Keio collection (***Datsenko and Wanner, 2000***; ***Baba et al., 2006***)), we only considered the MG1655 size data. The length and width measurements were well described by 0.5 $e^{1.09\cdot\lambda}$ + 1.76 μ m, and 0.64 $e^{0.24\cdot\lambda}$ μ m, respectively. In order to estimate cell size we take the cell as a cylinders with two hemispherical ends (***Si et al., 2017***; ***Basan et al., 2015***). Specifically, cell size (or volume) is estimated from,

$$V = \pi \cdot r^2 \cdot (l - 2r/3), \tag{4}$$

where r is half the cell width. A best fit to the data is described by 0.533 $e^{1.037\cdot\lambda}$ μ m^3. Calculation of the cell surface area is given by,

$$S = \eta \cdot \pi (\frac{\eta \cdot \pi}{4} - \frac{\pi}{12})^{-2/3} V^{2/3}, \tag{5}$$

where η is the aspect ratio ($\eta = l/w$) (***Ojkic et al., 2019***).

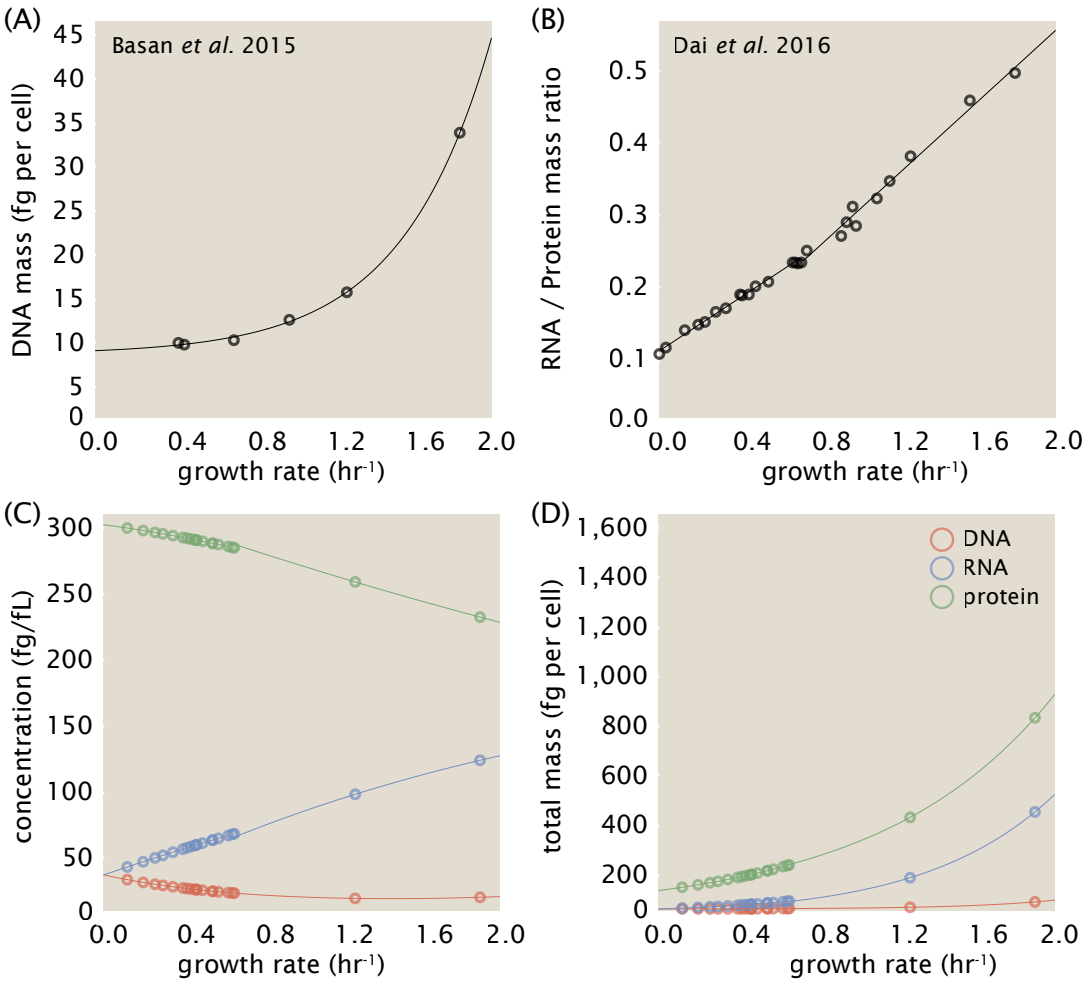

Figure 3. Empirical estimate of cellular protein, DNA, and RNA as a function of growth rate. (A) Measured DNA mass per cell as a function of growth rate, reproduced from Basan *et al.* 2015. The data was fit to an exponential curve (DNA mass in fg per cell is given by 0.42 $e^{2.23 \cdot \lambda}$ + 7.2 fg per cell, where λ is the growth rate in hr^{-1}). (B) RNA to protein measurements as a function fo growth rate. The data was for to two lines: for growth rates below 0.7 hr^{-1}, the RNA/protein ratio is $0.18 \cdot \lambda + 0.093$, while for growth rates faster than 0.7 hr^{-1} the RNA/protein ratio is given by $0.25 \cdot \lambda + 0.035$. For (A) and (B) cells are grown under varying levels of nutrient limitation, with cells grown in minimal media with different carbon sources for the slowest growth conditions, and rich-defined media for fast growth rates. (C) Predictions of cellular protein, DNA, and RNA concentration. (D) Total cellular mass predicted for protein, DNA, and RNA using the cell size predictions from Si *et al.*

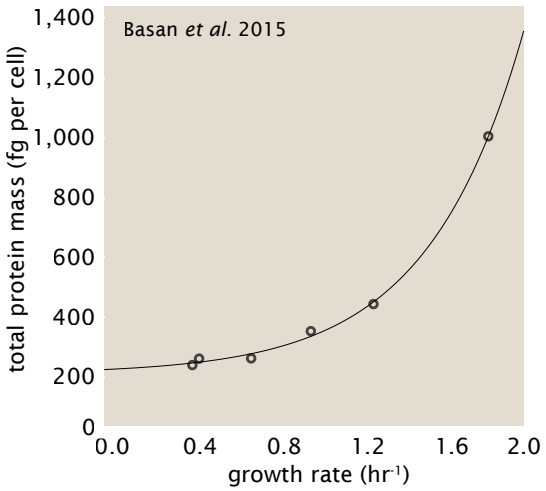

Figure 4. Total cellular protein reported in Basan *et al.* 2015. Measured protein mass as a function of growth rate as reproduced from Basan *et al.* 2015, with cells grown under different levels of nutrient limitation. The data was fit to an exponential curve where protein mass in fg per cell is given by 14.65 $e^{2.180 \cdot \lambda}$ + 172 fg per cell, where λ is the growth rate in hr^{-1}).

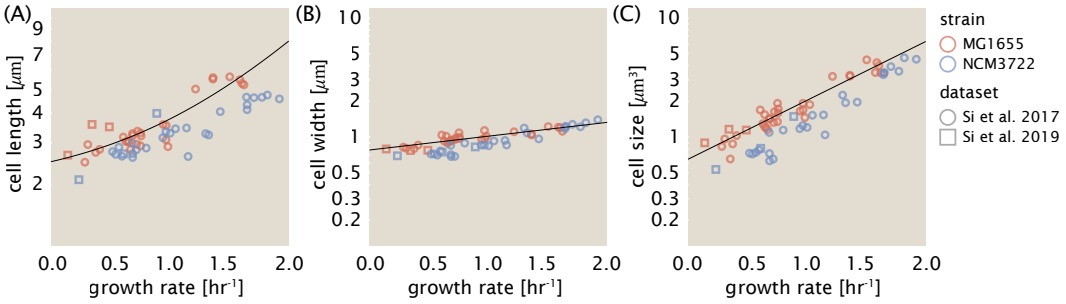

Figure 5. Summary of size measurements from Si *et al.* 2017, 2019. Cell lengths and widths were measured from cell contours obtained from phase contrast images, and refer to the long and short axis respectively. (A) Cell lengths and (B) cell widths show the mean measurements reported (they report 140-300 images and 5,000-30,000 for each set of samples; which likely means about 1,000-5,000 measurements per mean value reported here since they considered about 6 conditions at a time). Fits were made to the MG1655 strain data; length: 0.5 $e^{1.09 \cdot \lambda}$ + 1.76 μ m, width: 0.64 $e^{0.24 \cdot \lambda}$ μ m. (C) Cell size, V, was calculated as cylinders with two hemispherical ends (Equation 4). The MG1655 strain data gave a best fit of 0.533 $e^{1.037 \cdot \lambda}$ μ m^3.

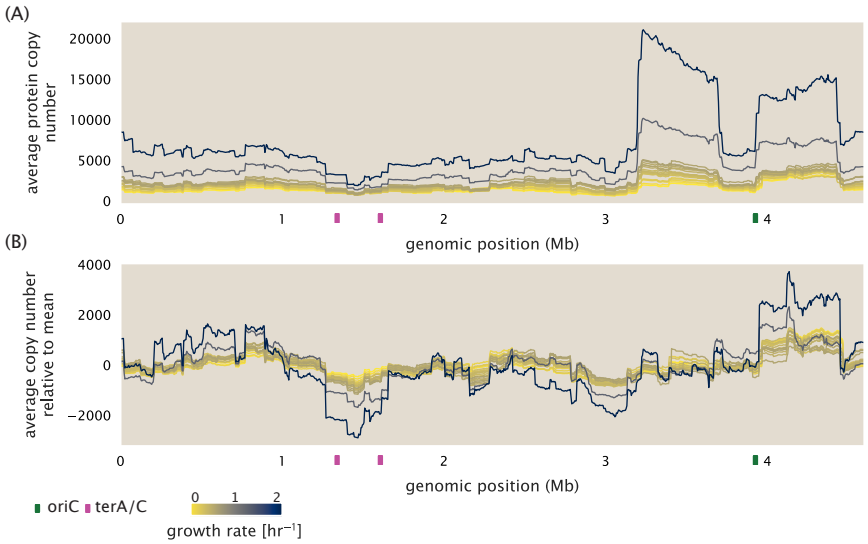

Figure 6. Position-dependent protein expression at different growth rates. (A) Protein copy number is reported along the length of the chromosome using a boxcar averaging, with window size of 0.5 Mb. (B)The boxcar average protein copy number, shifted relative to the mean value for each growth conditions, is show for a window size of 0.5 Mb. In this plot, all ribosomal proteins and elongation factor EF-Tu were excluded in the analysis.

Average protein expression across the chromosome.

In Figure 7(B) of the main text we plotted the average protein copy number along *E. coli*'s chromosome using a boxcar averaging (i.e. running average) window of 0.5 Mb. This means that at each position on the chromosome, proteins with a transcription start site that were +/- 0.25 Mb from that position were included in the calculated average. For *E. coli*, position 0 bp does not correspond the location of the origin and we keep to this convention, using the reported positional information from EcoCyc. Since the chromosome is circular, when calculating the average at positions near the end positions (i.e. near either 0 bp or 4.6 Mb) we include the copy numbers on opposing ends. For example, calculating the average for position 0 bp would include the range from 4.1 Mb to 0.25 Mb). Here we provide some additional analysis to show how the absolute copy numbers compare across growth conditions, as well as the effect of the specific averaging window size.

In the main text we centered each data set according to the mean average in order to compare the relative changes in copy number along the length of the chromosome in each data set. In reality, there is also a correlation between the total genomic content and protein copy number, which increases at faster growth. This is shown in Figure 6(A), where we plot the boxcar average from each growth condition without rescaling each about their mean values.

One of the challenges in interpreting this analysis is that the protein copy numbers for a small subset of proteins vary dramatically as a function of growth rate. This is particularly true for ribosomal proteins. In order to check whether the result is due simply due to the change in ribosomal copy number, we repeated the analysis with all ribosome proteins, and the translation elongation factor EF-Tu removed (Figure 6(B)). Indeed we still see a skew in protein abundance, with higher overall expression at the origin.

The other important parameter in this analysis is the size of the averaging window, which we took at 0.5 Mb. In Figure 7 we show the results when using averaging window sizes of 0.05 Mb, 0.25 Mb, 0.5 Mb, 1 Mb, and 2 Mb. Aside from the smallest window size of 0.05 Mb, the analysis seems to show a similar result, with proteins near the origin showing highest expression. For the window size of 0.05 Mb, the copy numbers become much noisier due to the large differences in protein copy number that are observed irrespective of the specific growth rate.

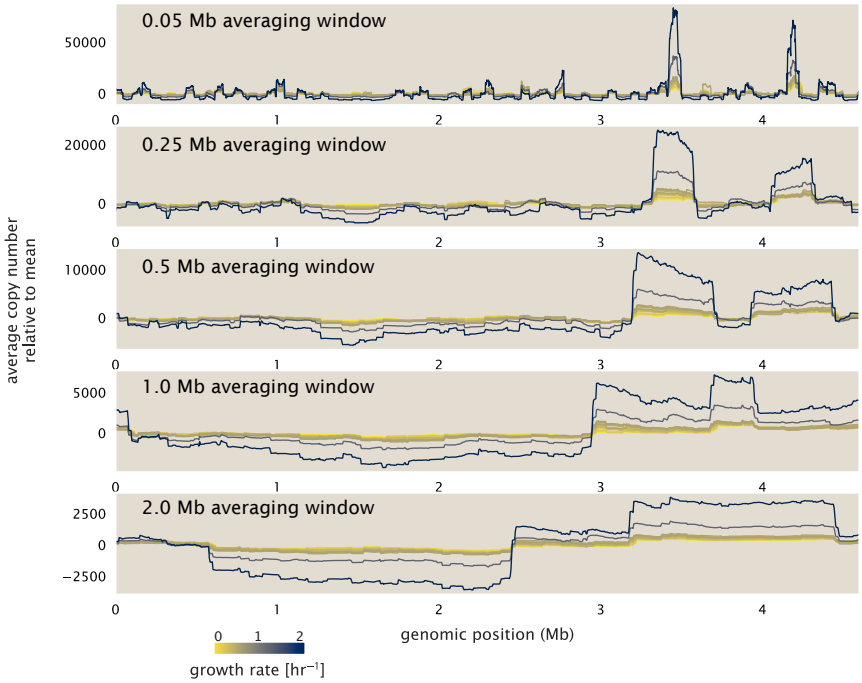

Figure 7. Position-dependent protein expression at different growth rates. (A) Protein copy number is reported along the length of the chromosome using a boxcar averaging. Here we consider different averaging window sizes: 0.05 Mb, 0.25 Mb, 0.5 Mb, 1.0 Mb, and 2 Mb.

Estimation of ⟨#ori⟩ / ⟨#ter⟩ and ⟨#ori⟩.

In the main text we consider the possibility that cells are varying their chromosomal content in order to increase ribosomal content, which will otherwise become limiting due to the maximal rRNA production per rRNA gene copy. While it is difficult to show a causal relationship, under such a scenario we nonetheless expect the ribosomal content to vary with the particular state of DNA replication. In particular, we can expect that the ⟨#ori⟩ / ⟨# ter⟩ ratio will reflect the skew in gene dosage for genes near the origin and therefore should relate to the relative abundance of ribosomes that are present closer to the origin. ⟨#ori⟩ is also useful to consider since it will reflect the total DNA content in the cell and therefore should relate to the total ribosomal abundance.

In order to estimate the ⟨#ori⟩ / ⟨# ter⟩ ratio, and ⟨#ori⟩, we made use of the measurements from Si *et al.* (2017). We consider their measurements of DNA replication time (t_C, 'C' period of cell division), total cell cycle time (t_{cyc}, 'C' + 'D' period of cell division), and doubling time τ from wild-type *E. coli* growing across a range of growth conditions.

We begin by considering ⟨#ori⟩. If the cell cycle time takes longer than the time of cell division, the cell will need to initiate DNA replication more often than its rate of division, $2^{\lambda t} = 2^{ln(2)\cdot t/\tau}$. Cells will need to do in in proportion to the ratio $\lambda_{cyc}/\lambda = t_{cyc}/\tau$, and the average number of origins per cell is then given by $2^{t_{cyc}/\tau}$. The average number of termini will in contrast depend on the lag time between DNA replication and cell division, t_D, with ⟨#ori⟩ / ⟨# ter⟩ ratio = $2^{t_{cyc}/\tau - t_D/\tau} = 2^{t_C/\tau}$.

In Figure 9(A) and (B) we plot the measured t_C and t_{cyc} values versus the doubling time from Si *et al.* data. The authors estimated t_C by marker frequency analysis using qPCR, while $t_{cyc} = t_C + t_D$ were inferred from t_C and τ. In the plots we see that both t_C and t_{cyc} reach a minimum at around 40 and 75 minutes, respectively. For a C period of 40 minutes, this would correspond to a maximum rate of elongation of about 1,000 bp/sec. Since we lacked a specific model to describe how each of these parameters vary with growth condition, we assumed that they were linearly dependent on the doubling time. For each parameter, t_C and t_{cyc}, we split them up into two domains corresponding to poorer nutrient conditions and rich nutrient conditions ($\tau \approx 55$ minutes). The fit lines are shown as solid black lines. In Figure 9(C) and (D) we also show t_C and t_{cyc} as a function of growth rate λ along

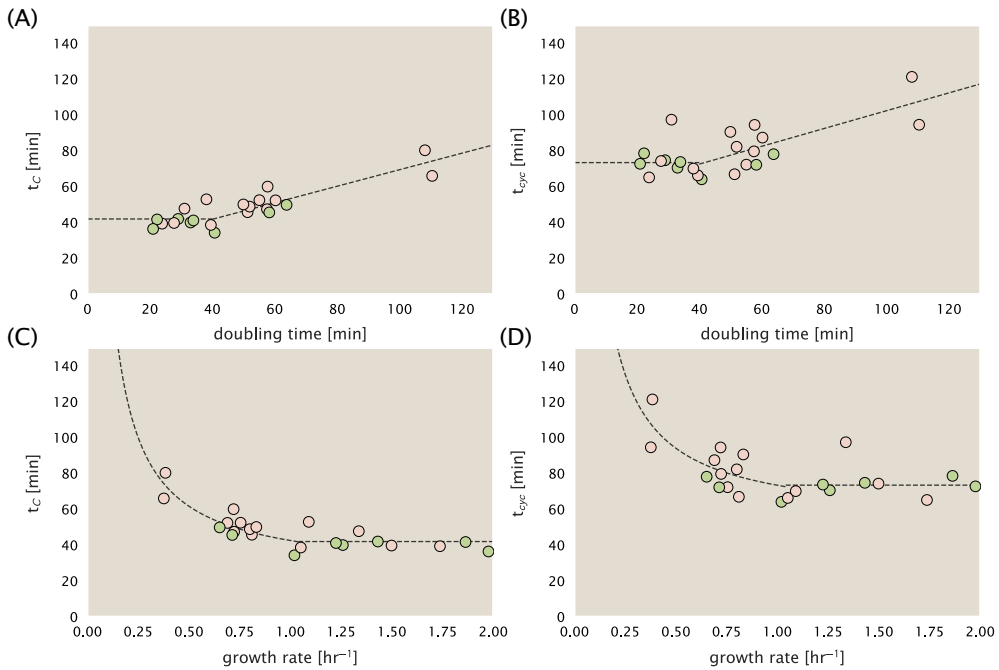

Figure 8. Estimation of ⟨#ori⟩ / ⟨# ter⟩ and ⟨#ori⟩ using data from Si *et al.* (2017). (A) and (B) plot the reported t_C and t_{cyc} as a function of cell doubling time τ, respectively. The dashed lines show a piecewise fit to the data. For short doubling times (rich media), t_C and t_{cyc} are assumed constant. At the transition, taken to occur at 40 minutes, the dashed line corresponds to an assumed proportional increase in each parameter as a function of the doubling time. (C) and (D) plot the same data as in (A) and (B), but as a function of growth rate, given by $\lambda = ln(2)/\tau$.

with our piecewise linear fits, which match the plots in the main text.

Hypothesis for increase in ribosomal abundance in the presence of chloramphenicol.

In the main text we note that the observed increase in ribosomal abundance upon addition of non-lethal concentrations of chloramphenicol may in part be a consequence of limiting rRNA production. Specifically, the proposal assumes that RNA polymerase are producing rRNA at their maximal rate (i.e. maximal packing of RNA polymerase on each rRNA operon). By sequestering ribosomes there will be a decrease in protein synthesis rate (i.e. lower $r_t \cdot \boldsymbol{R}$) and a corresponding increase in doubling time. Qualitatively then, we may then expect that that more rRNA (and therefore more ribosomes) may be produced for a specific growth condition and longer doubling times Figure 9(A).

Here we consider data from Si *et al.* (2017) where cells were grown in the presence of sub-lethal levels of chloramphenicol. In Figure 9(B) we plot measured RNA-to-protein ratios as a function of ⟨#ori⟩ / ⟨# ter⟩ (calculated using their reported values of τ_C and τ). While the data is relatively noisy, we do see that increasing concentrations of chloramphenicol is associated with an increased RNA-to-protein ratios and this appears roughly independent of the particular ⟨#ori⟩ / ⟨# ter⟩ ratio.

One challenge in interpreting the data is that the ⟨#ori⟩ / ⟨# ter⟩ ratio for a specific growth condition tends to decrease with increasing concentrations of chloramphenicol (indicated by marker type). Since the ⟨#ori⟩ / ⟨# ter⟩ ratio is defined by the ratio τ_C/τ, this is likely a reflection of chloramphenicol slowing down protein production relative to the rate of DNA replication (though, both τ_C and τ increase with added chloramphenicol).

Lastly, using the reported cell size data that was also available, we also consider how total ribosome copy number varies with growth condition and chloramphenicol. Here, as a first approaximation we assume that the total protein per cell will is proportional to cell size (with total protein ≈ cell volume x 1.1 g/ml x 30% dry mass x 55% protein). We then estimate the number of ribosomes

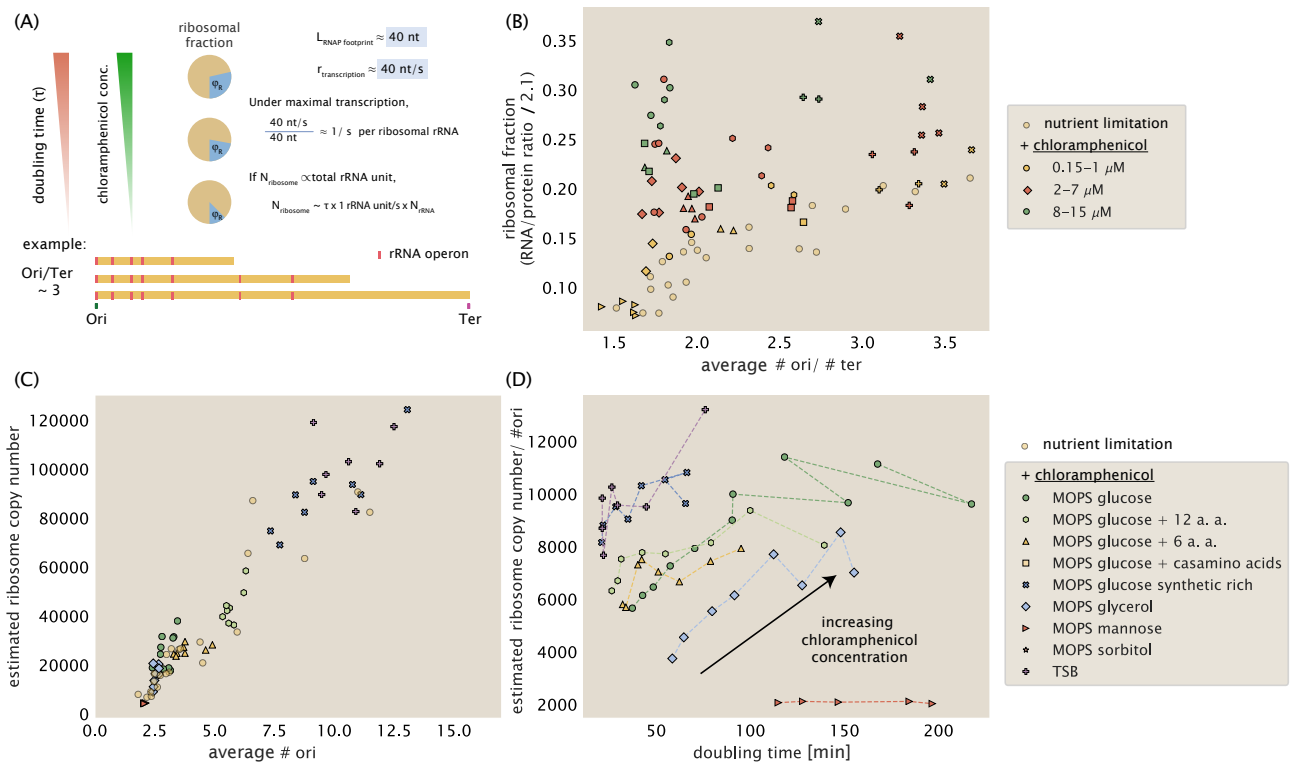

Figure 9. Potential effect of chloramphenicol on ribosomal abundance of if rRNA production is limiting. (A) Schematic of proposed change in ribosomal abundance upon addition of non-lethal does of chloramphenicol. We consider, for example, a ⟨#ori⟩ / ⟨#ter⟩ ratio of 3, which reflects an effective chromosome whose gene dosage is biased more so to regions near the origin. If ribosome production is limited by rRNA production in particular, then sequestering ribosomes will slow down cell doubling and provide addition time for more rRNA to be made. (B) Estimated ribosomal fraction (≈ RNA/protein ratio x 2.1 ***Dai et al.*** (***2016***)) at as a function of measured ⟨#ori⟩ / ⟨# ter⟩ ratio. Data is split into 'nutrient-limited' growth (pale yellow), low chloramphenicol concentration (yellow, 0.15 - 1 μM), medium chloramphenicol concentration (red, 2 - 7 μM), and high chloramphenicol concentration (red, 8 - 15 μM). Marker type corresponds to the growth media as indicated in part (C). (C) Scaling of estimated ribosomal copy number with ⟨#ori⟩, showing that cells still scale their total protein in accord with apparent growth law (***Si et al., 2017***) irrespective of presence of chloramphenicol. (D) Estimated ribosomal copy number normalized by ⟨#ori⟩. Data shows a media-specific increase in ribosomal abundance per origin with longer doubling times. All data is from (***Si et al., 2017***), and show that average values from each growth condition and chloramphenicol concentration (including data from both strains, MG1655 and NCM3722).

by multiplying the protein mass by our estimate of the ribosomal fraction. Consistent with the apparent generality in how growth relates to cell size (size ∝ ⟨#ori⟩) (***Si et al., 2017***), the number of ribosomes per cell collapse onto a roughly linear trend with respect to the ⟨#ori⟩ (Figure 9(C)).

That each of the chloramphenicol curves do not collapse onto a single line when normalized relative to ⟨#ori⟩ (Figure 9(D)) may be a reflection of biosynthetic rates increasing overall in richer media. For protein translation specifically, the rate of translation increases in both nutrient-limitation (***Scott et al., 2010***), and with increasing concentrations of chloramphenicol (***Dai et al., 2016***) for poorer media (up to maximum of about 17 aa per second). It may be that other processes, and production of rRNA in particular may also slow down in poorer media.

Calculation of active ribosomal fraction.

In the main text we estimate the fraction f_a of actively translating ribosomes across the different datasets available based on the growth-rate dependent measurements from the work of (***Dai et al., 2016***). Here we provide additional details on how f_a was initially determined, and how we have used it to estimate the active ribosomal fraction for each data set.

In the work of (***Dai et al., 2016***), the authors independently measured the translation rate, ribosomal abundance (via the total RNA-to-protein ratio), and growth rate λ across a vast range of growth conditions (growth rates spanning 0 - 2 h^{-1}). By requirements of mass balance, and

an assumption that cells are doubling their proteome with each cell division under steady-state growth, we expect,

$$r_t \cdot R\lambda \cdot N_{aa}. \tag{6}$$

r_t is the translation elongation rate, R is the number of ribosomes, and N_{aa} is the number of peptide bonds that must be formed to double the cell's protein mass. An important observation from the work of (***Dai et al., 2016***) was that their measured translation rates and ribosomal abundance were incompatible with this expectation. This was particularly true at slow growth (below about 0.7 h^{-1}). The explanation arrived at by the authors is that cells are regulating the fraction of ribosomes that are translating. As further support for this idea, sublethal concentrations of chloramphenicol caused a further decrease in the apparent fraction of actively translating ribosomes.

In Figure X we show the reported values of f_a as a function of growth rate in order to maintain $\cdot R \cdot f_a \; N_{aa} This corresponds to Equation 3 in the main text, where the$ estimate the fraction

References

Baba, T., Ara, T., Hasegawa, M., Takai, Y., Okumura, Y., Baba, M., Datsenko, K. A., Tomita, M., Wanner, B. L., and Mori, H. (2006). Construction of Escherichia coliK-12 in-frame, single-gene knockout mutants: the Keio collection. *Molecular Systems Biology*, 2(1):2460.

Basan, M., Zhu, M., Dai, X., Warren, M., Sévin, D., Wang, Y.-P., and Hwa, T. (2015). Inflating bacterial cells by increased protein synthesis. *Molecular Systems Biology*, 11(10):836.

Dai, X., Zhu, M., Warren, M., Balakrishnan, R., Patsalo, V., Okano, H., Williamson, J. R., Fredrick, K., Wang, Y.-P., and Hwa, T. (2016). Reduction of translating ribosomes enables Escherichia coli to maintain elongation rates during slow growth. *Nature Microbiology*, 2(2):16231.

Datsenko, K. A. and Wanner, B. L. (2000). One-step inactivation of chromosomal genes in Escherichia coli K-12 using PCR products. *Proceedings of the National Academy of Sciences*, 97(12):6640–6645.

Ojkic, N., Serbanescu, D., and Banerjee, S. (2019). Surface-to-volume scaling and aspect ratio preservation in rod-shaped bacteria. *eLife*, 8:642.

Schaechter, M., MaalØe, O., and Kjeldgaard, N. O. (1958). Dependency on Medium and Temperature of Cell Size and Chemical Composition during Balanced Growth of Salmonella typhimurium. *Microbiology*, 19(3):592–606.

Scott, M., Gunderson, C. W., Mateescu, E. M., Zhang, Z., and Hwa, T. (2010). Interdependence of cell growth and gene expression: origins and consequences. *Science*, 330(6007):1099–1102.

Si, F., Li, D., Cox, S. E., Sauls, J. T., Azizi, O., Sou, C., Schwartz, A. B., Erickstad, M. J., Jun, Y., Li, X., and Jun, S. (2017). Invariance of Initiation Mass and Predictability of Cell Size in Escherichia coli. *Current Biology*, 27(9):1278–1287.

Taheri-Araghi, S., Bradde, S., Sauls, J. T., Hill, N. S., Levin, P. A., Paulsson, J., Vergassola, M., and Jun, S. (2015). Cell-size control and homeostasis in bacteria. *Current Biology*, 25(3):385–391.

Volkmer, B. and Heinemann, M. (2011). Condition-Dependent Cell Volume and Concentration of Escherichia coli to Facilitate Data Conversion for Systems Biology Modeling. *PLOS ONE*, 6(7):e23126.

You, C., Okano, H., Hui, S., Zhang, Z., Kim, M., Gunderson, C. W., Wang, Y.-P., Lenz, P., Yan, D., and Hwa, T. (2013). Coordination of bacterial proteome with metabolism by cyclic AMP signalling. *Nature*, 500(7462):301–306.